Malaysian Journal of Analytical Sciences (MJAS)
Published by Malaysian Analytical Sciences Society

UNVEILING ZN/NI/CO TERNARY MIXED TRANSITION METAL OXIDES COMPOSITE ANCHORED ON GRAPHENE OXIDE AS A POTENTIAL MATERIAL FOR SUPERCAPACITOR ELECTRODE

(Menyingkap Potensi Komposit Logam Peralihan Zn/Ni/Co yang Terikat pada Grafin Oksida sebagai Elektrod Superkapasitor)

Nurul Infaza Talalah Ramli[1,2], Ab Malik Marwan Ali[1,2,3*], Nur Hafiz Hussin[1], Mohamad Fariz Mohamad Taib[1,3] and Oskar Hasdinor Hassan [1,3]

[1]*Faculty of Applied Sciences, Universiti Teknologi MARA, 40450 Shah Alam, Selangor, Malaysia*
[2]*Faculty of Applied Sciences, Universiti Teknologi MARA, 26400 Bandar Tun Abdul Razak Pahang, Malaysia*
[3]*Institute of Sciences, Universiti Teknologi MARA, 40450 Shah Alam, Selangor, Malaysia*

[*]*Corresponding author: ammali@uitm.edu.my*

Received: 14 September 2023; Accepted: 11 June 2024; Published: 27 August 2024

Abstract

Ternary metal oxides continue to draw noteworthy research interest among the energy storage society owing to their remarkable attributes such as upstanding storage capability and cost-effectiveness. Despite that, reduced electrical conductivity and capacity instability tend to hamper the applicability of ternary metal oxides. This work reports a feasible approach to enhance the supercapacitive potential of ternary metal oxide (Zn-Ni-CoO) by incorporating graphene oxide (GO) conductive network. The structural, morphology, and functional groups were deduced via XRD, FESEM, EDS elemental mapping, FTIR, and BET analysis. The metal-carbon hybrid shows astounding specific capacitance value of 608 Fg^{-1} at 5 mVs^{-1}, calculated from three-electrode cyclic voltammetry analysis, with 2 M KOH electrolyte. Significantly, the material is able to preserve 93% of its initial capacitance even after 1000 cycles. This performance is ascribed to the synergistic effect generated by the electric double layer capacitance (EDLC) properties of GO and pseudocapacitance behavior originated from Zn-Ni-CoO. Based on the research findings, Zn-Ni-Co/GO nanocomposite could serve as a favorable active material for supercapacitor electrode.

Keywords: zinc-nickel-cobalt oxide, graphene oxide, electrochemical performance, specific capacitance, supercapacitor

Abstrak

Gabungan tiga elemen logam oksida telah menarik minat para komuniti penyelidik dalam bidang penyimpanan tenaga kerana sifatnya yang luar biasa seperti kemampuan penyimpanan yang tinggi serta keberkesanan kos. Walaupun begitu, kekonduksian elektrik yang berkurang dan ketidakstabilan kapasiti cenderung menghalang penggunaan oksida logam terner. Karya ini melaporkan pendekatan yang wajar untuk meningkatkan potensi superkapasitor logam oksida terner (Zn-Ni-Co O) dengan menggabungkan rangkaian konduktif grafin oksida (GO). Sifat struktur, morfologi, dan fungsional bagi bahan ini disimpulkan melalui analisis XRD, FESEM, EDS-elemen pemetaan, FTIR, dan BET. Hibrid logam-karbon menunjukkan nilai muatan kapasiti spesifik yang setinggi 608 Fg^{-1} pada 5 mVs^{-1}, yang dikira dari analisis voltammetri siklik tiga-elektrod, dengan elektrolit 2 M KOH. Secara keseluruhannya, bahan ini dapat mengekalkan 93% kapasitansi awalnya walaupun selepas 1000 kitaran. Prestasi ini disebabkan oleh kesan sinergi yang dihasilkan oleh sifat kapasitansi lapisan dua elektrik (EDLC) yang datang daripada GO dan

kapasitan yang berasal dari Zn-Ni-Co O. Berdasarkan penemuan penyelidikan, Nanokomposit Zn-Ni-Co / GO boleh berfungsi sebagai bahan aktif yang baik untuk elektrod superkapasitor.

Kata kunci: zink-nikel-kobalt oksida, grafin oksida, prestasi elektrokimia, muatan spesifik, superkapasitor

Introduction

Transition metal oxide (TMO) nanoparticles exhibit distinctive characteristics in their chemical, thermal, optical, magnetic, and electrical properties, which differ from their bulk counterparts. TMO and their composites have been employed in a wide range of disciplines, including photocatalysis [1], sensors [2], and energy storage [3], [4]. The remarkable features of nanoparticles are governed by factors such as their size, structure, morphology, as well as the method of their production. When it comes to morphological aspects, the synthesis method of a nanoparticle plays a significant role in controlling its overall structure. There are great deal of methods that have been previously reported in preparing the hybrids of metal oxides, for instance hydrothermal [5] , solvothermal [6], combustion [7], co-precipitation [8], templated synthesis [9], microwave assisted [10], and sol-gel [11, 12]. Typically, Chen et al. synthesized an urchin-like $ZnCo_2O_4$ via a two-step synthetic route comprising of solvothermal and annealing process [13]. The resulting $ZnCo_2O_4$ are constructed from numerous porous nanorods, with diameters ranging from 80 to 200 nm. These microspheres exhibit a specific surface area of 28 $m^2 g^{-1}$. By altering the volume ratios of water to ethanol, it is possible to effectively manipulate the shapes of the resulting $ZnCo_2O_4$ samples. Meanwhile, Gao et al. implemented a facile hydrothermal method with subsequent calcination procedure to synthesis $NiCo_2O_4$ [14]. Consequently, an enhanced performance of micron-scale $NiCo_2O_4$ with distinct hollow fibrous structure was obtained. This improvement can be attributed to several factors, including a larger specific surface area, increased pore volume, and shorter diffusion path for both electrolyte ions and electrons. In another work conducted by Wei et al. sol-gel route was utilized to prepare $ZnCo_2O_4$ [15]. The obtained particle size was reported to range from 15-20 nm, slightly lower than the value documented in [13]. The synthesis of composite materials comprising mixed TMOs anchored on GO for supercapacitor electrodes has faced numerous obstacles in terms of analytical performance in prior research endeavors. Conventional methods like hydrothermal synthesis and direct chemical precipitation commonly lead to inadequate dispersion and aggregation of metal oxides on the surface of GO [16]. This leads to compromised electrochemical performance and limited charge transfer kinetics. Moreover, these methods often lack precise control over the composition and morphology of the TMO, potentially affecting the specific capacitance and cycling stability of the electrode material.

Specifically in energy storage implementation, TMO often plays an important role as it exhibits a remarkable capacitance. However, despite its promising energy density, TMO encounters obstacles such as low conductivity, uncontrolled volumetric changes, and sluggish ion diffusion within the bulk phase, which then impedes its practical and industrial utility. In general, the desirable characteristics for electrode materials in supercapacitors include excellent conductivity, a high specific surface area, notable thermal stability, significant mechanical strength, and high capacitance [17]. Consequently, there is a necessity to explore functional metal oxides with improved electrochemical properties for supercapacitor (SC) applications. Engineering strategies targeting the composition, fabrication, electroconductivity, and oxygen vacancies of metal oxide nanomaterials have successfully bolstered their inherent properties, encompassing enhancements in conductivity, surface area, stability, and active sites, among other factors. TMO primarily possesses a distinctive characteristic of hosting multiple distinct cations within a single crystalline structure. This coexistence of cations results in a higher number of available electrons compared to metal oxides composed of a single element, thus leading to improved electrical properties. For instance, spinel oxides such as $ZnCo_2O_4$ exhibits a conductivity that is two to three orders of magnitude greater than that of single Co_3O_4 constituent [18]. Simultaneously, carbon-accolades are commonly regarded as superior active materials for supercapacitors. Integration of TMO and carbons are proven to help prevent or minimize severe agglomeration and restacking of the hybrid structure

ensembles. As a result, a larger electrochemically active surface area becomes available, ultimately leading to enhanced electrochemical performance [19].

In this specific work, an effective facile synthesis route of Zn/Ni/Co (ZNC) ternary MTMO anchored on GO has been successfully developed. This technique offers numerous advantages compared to traditional methods. Firstly, it provides superior control over the composition and morphology of the ternary metal oxides by finely adjusting precursor ratios and reaction conditions. Secondly, the sol-gel process ensures the even dispersion and anchorage of metal oxides onto the graphene oxide surface, fostering efficient charge transfer and enhanced electrochemical performance. Furthermore, the co-precipitation stage facilitates the creation of mixed metal oxides with precisely defined crystal structures and heightened synergistic interactions among various metal components, potentially resulting in increased specific capacitance and superior cycling stability. To the best of our knowledge, there are no studies documenting the utilization of ternary MTMO comprising Zn/Ni/Co mixed with GO as active material for supercapacitor electrode. Hence, it is of great importance to study the effect of GO incorporation into the Zn/Ni/Co ternary MTMO.

Materials & Methods

Materials

All the chemicals utilized were used without any further modification. Co $(NO_3)_2{\cdot}6H_2O$, Zn $(NO_3)_2{\cdot}6H_2O$, Ni $(NO_3)_2{\cdot}6H_2O$ (98%) and oxalic acid (99%) were purchased from sigma Aldrich, graphene oxide powder from China Beiihai Building Material Co. LTD, whereas potassium hydroxide (85%) from R&M chemicals.

Preparation of Zn/Ni/Co Oxide-GO

In brief, appropriate amounts of starting materials consisted of Co $(NO_3)_2{\cdot}6H_2O$, Zn $(NO_3)_2{\cdot}6H_2O$, and Ni $(NO_3)_2{\cdot}6H_2O$ were dissolved separately in deionized water. Once the reagents were solvated, an appropriate amount of oxalic acid was added under continuous magnetic stirring at 80 ˚C up until the mixture turned into a gel-like substance. Further, the resulting gel was heated at 110 ˚C to ensure the formation of powder before subsequently being dried and ground. The sample was calcined at 350 ˚C for 3 h afterwards with a heating rate of 5 ˚C/min to acquire the desired ternary metal oxides composites. The procured Zn/Ni/Co Oxide sample (ZNC) was then used further for GO compositing.

Adequate amounts of ZNC powder were dissolved in deionized water and stirred for 30 minutes. In a separate beaker, GO was also dissolved in deionized water and sonicated for 30 minutes to achieve a homogenous solution. Both solutions were then poured together into one beaker and subjected to 24 hours stirring process. Ultimately, the resulting precipitates were gathered through centrifugation, subjected to multiple rinses with deionized water and ethanol, and then dried at 80 °C for a duration of 24 hours to yield the final products.

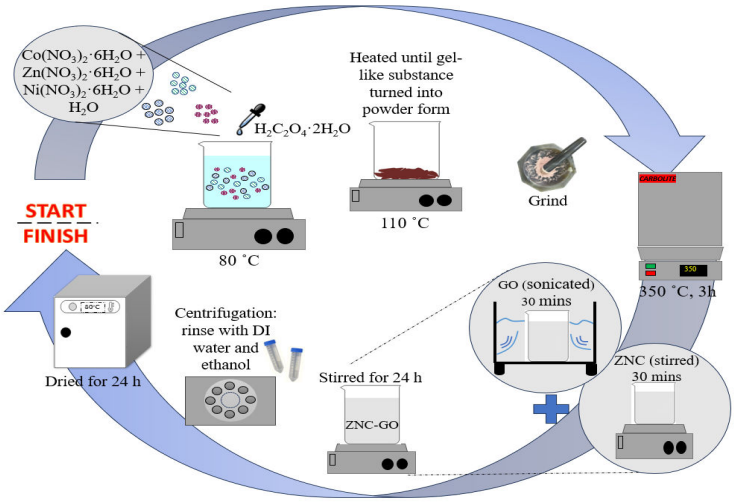

Figure 1. Methodology flowchart

Characterization

The compositions of the as-prepared samples were characterized using X-ray diffraction (XRD), whilst the morphologies and the microstructures of the samples were investigated by imagining with field-emission scanning electron microscope (FESEM) and energy dispersive spectroscopy (EDS) mapping analysis. The presence of chemical bonding was confirmed by Fourier transform infra-red (FTIR) spectroscopy in the range of 450 cm^{-1} – 4000 cm^{-1}. The specific surface area (SSA), pore width, and pore volume was deduced by Brunauer–Emmett–Teller (BET) and Barrett-Joyner-Halenda (BJH) measurements whereas the electrochemical measurements were conducted via a three-electrode system operated by an Autolab PGSTAT204N potentiostat. The setup was using a glassy carbon electrode (GCE) with drop-casted sample on its tip as the working electrode. Ag/AgCl served as the reference electrode while platinum wire was used as the counter electrode, with 2 M KOH as the electrolyte. Cyclic voltammetry was performed over the potential range of 0 – 0.6 V at various scan rates ranging from 20 – 100 mVs^{-1}.

Results and Discussion

X-ray diffraction analysis

XRD analysis was carried out to study the phase structure and the sample's degree of crystallinity. Evident from Figure 2, both ZNC and ZNC-GO samples display a very similar pattern, suggesting that the incorporation of GO does not significantly alter the bulk crystal structure or phase composition of ZNC. The diffraction peaks can be ascribed to the crystallographic data JCPDS no 03-065-3103, with no excrescent peaks detected. The findings indicate a complete conversion of all precursors into pure spinel ternary Zn/Ni/Co O and Zn/Ni/Co-GO nanocomposites. The peak positions are listed in Table 1, with eight apparent peaks indexed to (111), (220), (311), (400), (422), (511), (440), and (533) diffraction planes. Also, a weak diffraction peak at 2θ = 11.09˚ corresponds to (001) diffraction plane due to a very small amount of GO addition and the presence of oxygen functional group [20]. The weak and almost unnoticeable peak is also inferring to the random orientation nature of GO, and high loading mass of ZNC [21]. The resemblance in peak positions seen on both ZNC and ZNC-GO with the stick pattern implies that both samples retain a similar spinel cubic structure. The crystallite sizes and lattice constant can be deduced by implementing Debye Scherrer formulation (Eq.1) and Eq.2, respectively.

$$D = \frac{k\lambda}{\beta cos cos\ \theta} \quad (1)$$

$$a = D\ (h^2 + k^2 + l^2\ )^{\frac{1}{2}} \quad (2)$$

In which D is the crystallite size (nm), k is the Scherrer constant, λ represents the wavelength of the x-ray source, β symbolizes the full width at half maximum (FWHM) of the diffraction peak, θ is the peak positions, and hkl refers to the miller indices. The specific FWHM, crystallite size, and cell parameters of ZNC and ZNC-GO are detailed in Table 2. Based on the displayed data, it is evident that the crystallite size and lattice parameter obtained at the most intense peak (311) for ZNC-GO are slightly below ZNC. The energy storage capacity is significantly influenced by the size and dimension of the crystallites, hence reflecting the material's level of electrical conductivity

.

Table 1. The peak positions in XRD patterns of samples

Samples	(111)	(220)	(311)	(400)	(422)	(511)	(440)	(533)
ZNC	19.16	31.33	36.89	44.60	55.39	59.18	65.00	77.18
ZNC-GO	19.23	31.40	37.07	44.83	55.57	59.52	65.18	77.54
JCPDS 03-065-3103	19.07	31.38	36.98	44.97	55.87	59.58	65.49	77.66

Table 2. The FWHM, estimated crystallite size, and cell parameter of ZNC and ZNC-GO using XRD spectra

Samples	(311) Peak Position, 2θ (°)	FWHM (Rad.)	Crystallite Size, d (nm)	Cell Parameter a=b=c, (Å)	Cell Parameter a=b=c, (Å) from Literature
ZNC	36.89	0.79952	10.48	8.063	8.107 [3]
ZNC-GO	37.07	1.33929	6.26	8.043	-

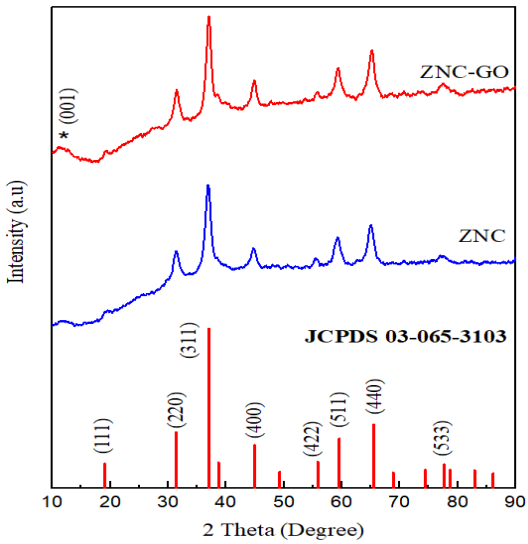

Figure 2. XRD patterns of ZNC and ZNC-GO

Field emission scanning electron microscopy

The morphology of ZNC and ZNC-GO were investigated via FESEM. The image obtained shows heterogenous morphologies considering the hybrid nature of the samples. ZNC micrograph in Figure 3 (a) displays a mixture of petal-like, and sphere-like shapes in various sizing clustered together. These three different elements show different identity shapes, each corresponding to Zn, Ni, and Co elements. Meanwhile, the FESEM image of sample with GO in Figure 3 (b) shows an interesting, wrinkled cabbage-like shape which is believed to be the GO sheet, with fine particles clusters anchored on its surface indicating the attachment of ZNC. The cabbage-like morphology is in good agreement with the FESEM GO-based nanocomposite result documented by Iranshahi & Mosivand [22]. It is also evident that the spherical particles in ZNC are more agglomerated compared to ZNC-GO. These are probably because TMO nanoparticles have high surface energy and attractive forces between particles, which causes them to clump together. When GO is added into the TMO matrices, it acts as a spacer that prevents direct contact between nanoparticles, thus reducing agglomeration. Figure 3 (c) shows the energy dispersive spectroscopy (EDS) mapping analysis, disclosing a congruent distribution of Zn, Ni, Co, O, and C throughout the ZNC-GO structure. This implies a successful synthesis route of ZNC-GO.

Fourier transform infrared

FTIR analysis provides a valuable insight into the functional groups and intermolecular interactions by examining the stretching or bending vibrations of specific bonds. Figure 4 presents the FTIR spectra of ZNC and ZNC-GO with the magnified version presented on the inset. The ZNC-GO retains the same band spectra exhibited by ZNC with a slight shift, owing to their shared MTMO composition with just a dash of GO added. The sharp bands which appear at 648 cm^{-1} and 553 cm^{-1} for ZNC sample whilst at 655 cm^{-1} and 550 cm^{-1} for ZNC-GO are corresponding to metal-oxygen bond [23]. For ZNC, the band arises at 1323 cm^{-1} and 1611 cm^{-1} representing the organic and water molecules, as well as hydroxide ions [6]. The FTIR spectra shown by ZNC-GO displays more distinctive peaks compared to ZNC. The band appears at around 1300 cm^{-1} is

ascribable to the presence of C-O [24]. At ~3800 cm^{-1}, the band is formed due to the stretching vibrations of hydroxyl group [25]. Weak signal at 2100 cm^{-1} is probable to the aliphatic C-H stretching [26]. Furthermore, the IR band appears in 1708 is correlated with the stretching vibration of sp^2 hybridized C=C [27].

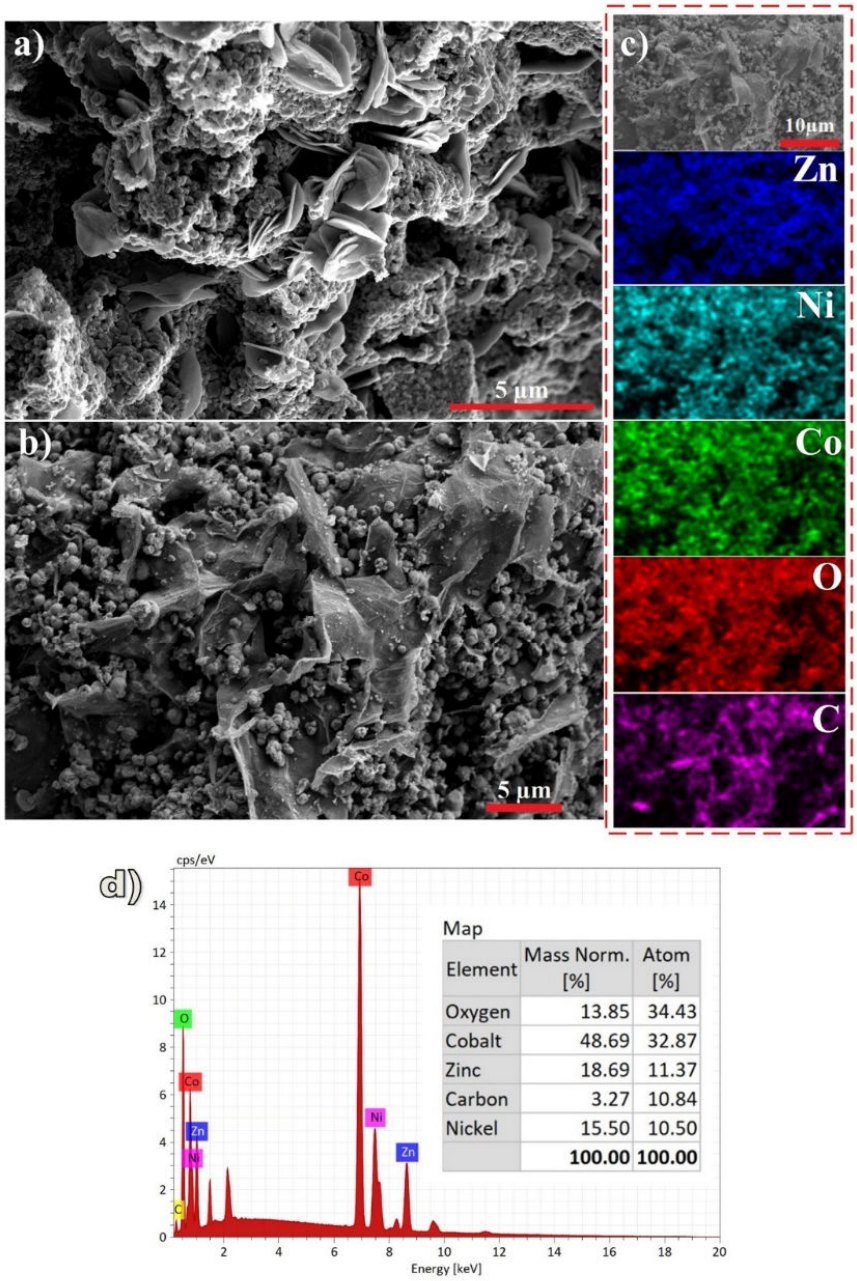

Figure 3. FESEM images of (a) ZNC, (b) ZNC-GO, (c) elemental mapping of ZNC-GO, and (d) EDS elemental peak of ZNC-GO

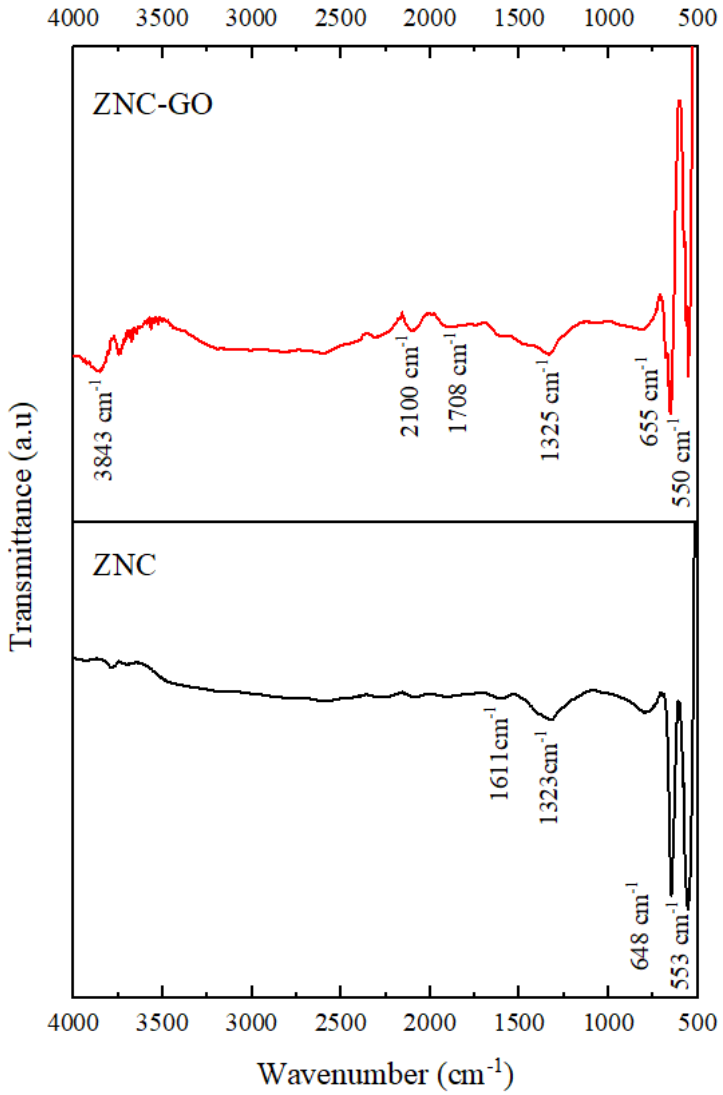

Figure 4. FTIR spectra of ZNC and ZNC-GO

Brunauer–Emmett–Teller

Figure 5 portrays the results of adsorption–desorption measurements, which were conducted to examine the specific surface area (SSA) and pore structure of ZNC-GO sample. The obtained nitrogen adsorption and desorption isotherm verifies the high porosity properties of the prepared metal-carbon nanocomposite. The resulting SSA of Zn/Ni/Co-Go is revealed to be 55.92 m^2 g^{-1}, comparable to the value reported in [28]. The high SSA value facilitates a significant amount of electrochemical active sites and enhances ion–electron interaction, hence leads to an improved electrochemical performance [29]. As displayed in figure 5, a distinct hysteresis loop resembling H3 type is evident, ranging from 0.39 – 1.0 relative pressure (p/p_o). Furthermore, the pore size distribution of ZNC-GO was explored by means of Barrett-Joyner-Halenda (BJH) method, as shown in the inset of Figure 5. The average pore diameter of ZNC anchored on GO sheets was observed from 2 – 6 nm, implying its mesoporous feature. Additionally, according to the measurements, the obtained pore volume for ZNC-GO is 0.1375 cm^3 g^{-1}. The obtained pore volume is slightly higher than the value reported in [30], which also happened to study the material's supercapacitive performance.

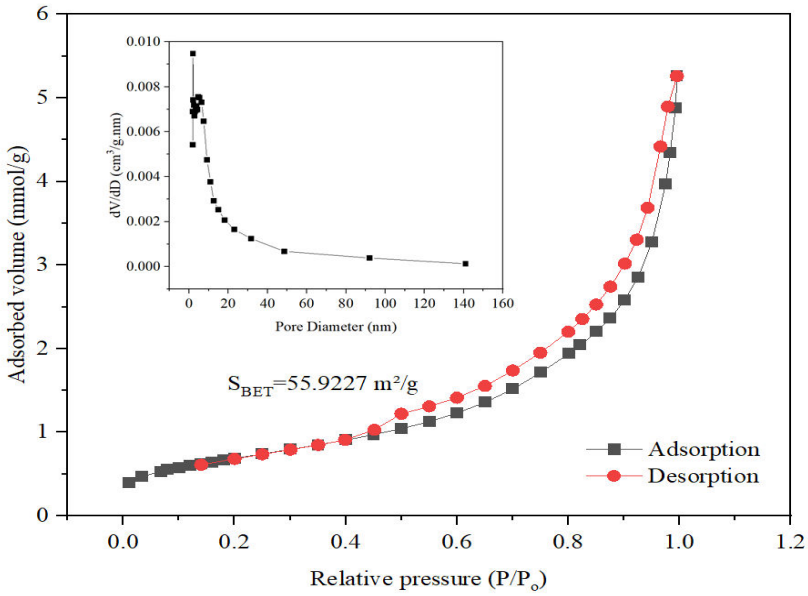

Figure 5. Nitrogen adsorption-desorption isotherm of ZNC-GO and the corresponding pore diameter distribution (inset)

Cyclic voltammetry

CV analysis was employed to analyze the specific capacitance (C_s) value of ZNC and ZNC-GO hybrid. The CV scans were recorded at numerous scan rates ranging from 5 to 100 mVs^{-1}, within the potential window of 0.0 to 0.6 V. Figure 6 (a) displays the CV curves comparison of ZNC and ZNC-GO samples at 50 mVs^{-1}. It is evident that ZNC-GO exhibits higher current response, as well as greater area under the CV curve compared to ZNC. ZNC curve shows a pair of prominent redox peaks, indicating its pseudocapacitive behavior [31]. With the inclusion of GO, vague appearance of redox peaks is witnessed. The broadening of redox peak demonstrates a significant increase of electron transfer and ion diffusion [32]. In Figure 6 (b), the voltammogram shows a progressive size as the scan rates increased. The highest current response can be seen on 100 mVs^{-1} curve while the lowest shown by 5 mVs^{-1}. The graphs show a stagnant shape at all scan rates, implying good electrochemical reversibility [33]. The C_s values were obtained by means of Eq 3.

$$C_s = \frac{\int_{v_a}^{v_c} IV(dV)}{vm\,(V_c - V_a)} \quad (3)$$

Based on the equation, C_s is the specific capacitance presented in the unit of Fg^{-1}. V_c and V_a indicate the potential window in volts, I(V) demonstrate the response current (A), v is the potential scan rates (Vs^{-1}), and m is the mass of sample drop-casted on the tip of the electrode (g). Upon calculation, the C_s value obtained for ZNC is 113 Fg^{-1} and 318 Fg^{-1} for ZNC-GO at 50 mVs^{-1}, with nearly threefold increment. Figure 6 (c) shows the calculated C_s trend for ZNC-GO sample at various scan rates. Contrast to the progressive pattern of CV curves displays on Figure 6 (b), the value calculated shows a declining trend as the scan rates increase, which is also depicted in Table 3. This pattern was instigated by a complete permeation of electrolyte ions at lower scan rates. Yet, the movement of electrolyte ions is somewhat restricted at higher scan rates due to time limitations [34]. The stability of the ZNC-GO sample was assessed by continuously running CV tests for 1000 cycles, as can be seen on figure 6 d). Based on the obtained data, ZNC-GO retains 93% of its initial C_s value, indicating excellent electrochemical stability.

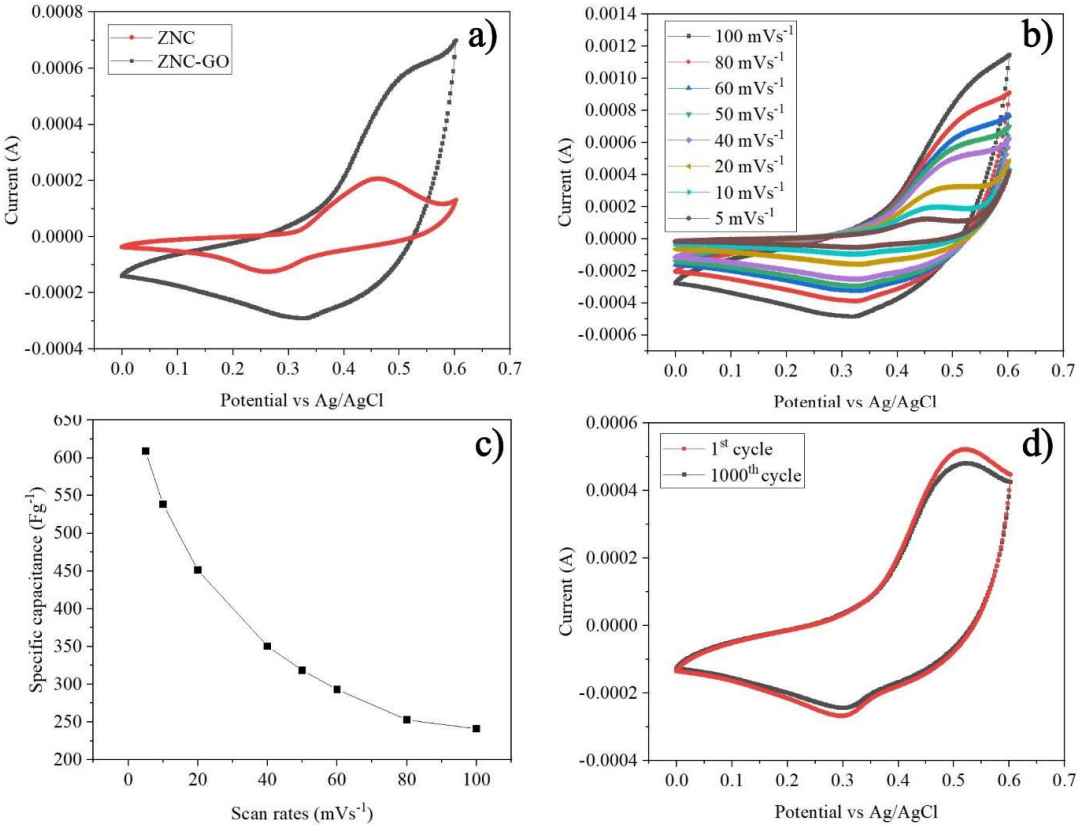

Figure 6. (a) CV curves of ZNC and ZNC-GO at 50 mVs^{-1}, (b) CV curves of ZNC-GO samples at various scan rates, and (c) The C_s trend for ZNC-GO at various scan rates, and (d) Stability test of ZNC-GO at 100 mVs^{-1}

Table 3. Specific capacitance of ZNC, ZNC-GO obtained in this work and other reports in previous works

Samples	Specific Capacitance, Cs (Fg^{-1})	Scan Rate or Current Density	Electrolyte	Reported by Literature
ZNC	113.76	50 mVs^{-1}		
ZNC-GO	240.92	100 mVs^{-1}		
ZNC-GO	252.90	80 mVs^{-1}		
ZNC-GO	292.90	60 mVs^{-1}		
ZNC-GO	318.38	50 mVs^{-1}	1 M KOH	This work
ZNC-GO	350.25	40 mVs^{-1}		
ZNC-GO	450.92	20 mVs^{-1}		
ZNC-GO	538.34	10 mVs^{-1}		
ZNC-GO	**608.86**	5 mVs^{-1}		
Graphene-$NiCo_2O_4$	266.00	2 mVs^{-1}	2 M KOH	[35]
$MgCo_2O_4$/graphene	189.00	5 mVs^{-1}	3 M KOH	[36]
GO/Chitosan/ZnO	137.70	0.5 Ag^{-1}	NA	[37]
Zn-Ni-Co/graphene	502.00	0.2 Ag^{-1}	2 M KOH	[38]

$NiCo_2O_4$ – nickel cobaltite
$MgCo_2O_4$ – magnesium cobaltite
ZnO – zinc oxide

Galvanostatic charge/discharge

Galvanostatic charge-discharge (GCD) is a reliable and efficient method to determine and evaluate the electrochemical capacitance performance of materials. A comparison of GCD curves at 10 Ag^{-1} for ZNC and ZNC-GO can be seen on Figure 7. It should be noted that ZNC-GO displays longer discharge time compared to ZNC, which also indicates higher C_s value [39]. Another vital parameter to determine the practical performance of supercapacitor material are energy density, E (Wh/kg) and power density, P (W/kg). Eq (4) and (5) indicate the equations for energy density and power density, respectively:

$$E = \frac{1}{2} CV^2 \quad (4)$$

$$P = \frac{E}{\Delta t} \quad (5)$$

At the current density of 10 Ag^{-1}, the energy density of ZNC was calculated to be 7.92 Wh/kg at a power density of 208.91 W/kg. The energy density was raised to 11.98 Wh/kg with power density of 382.67 W/kg once GO was incorporated into the ZNC MTMO composites. The GCD curves exhibit a distinct plateau region for every current density, along with a nearly symmetric shape. This behavior suggests that the electrode undergoes a reversible Faradaic redox reaction, demonstrating an ultralow energy loss or an exceptionally high coulombic efficiency. Furthermore, the symmetric nature of the GCD curves indicates ideal pseudocapacitive behavior, which is a desirable characteristic for high-performance energy storage devices [40]. This result is also in good agreement with the CV profile obtained in the previous section. The enhanced electrochemical performance of ZNC-GO can be attributed to the synergistic effect arising from the combination of ZNC ternary MTMO and GO sheet. This synergistic effect increases the number of available oxidation states and shortens the pathways for ion and electron transport. Moreover, the porous and high surface area nature of the composite material, facilitated by GO, provides abundant active sites for redox reactions and ion adsorption/desorption processes. These observations suggest that the ZNC-GO sample can be regarded as a potential electrode material for supercapacitors.

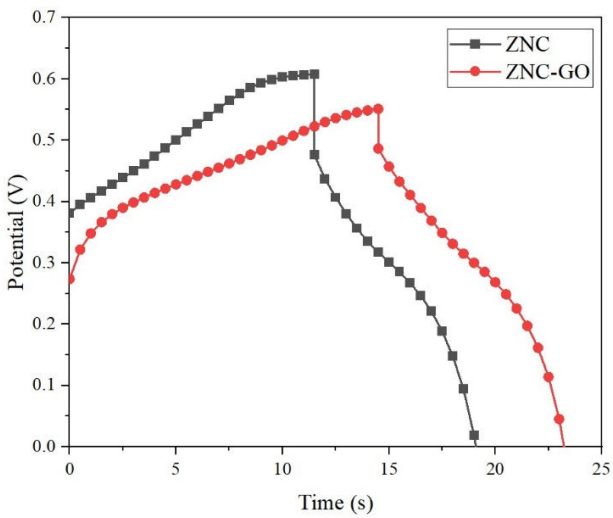

Figure 7. GCD curves of ZNC and ZNC-GO at 10 Ag^{-1}.

Conclusion

In summary, ZNC-GO with heterogenous morphology of flake-lake and sphere like small particles anchored on the cabbage-like sheet was successfully prepared via a facile sol-gel annealing synthesis route. Based on Scherrer's formulation, the estimated crystallite size of ZNC (10.48 nm) became smaller (6.26 nm) after GO addition, with SSA value as high as 55.92 m^2 g^{-1}. The synergistic interaction between high surface area GO and high theoretical capacities ZNC facilitates a significant amount of electrochemical active sites thus enhances ion–electron interaction. Subsequently,

through the integration of GO into the ZNC matrices, the C_s value intensified three-fold from 113 Fg^{-1} to 318 Fg^{-1} at 50 mVs^{-1}, with highest C_s value of 608 Fg^{-1} obtained at a scan rate of 5 mVs^{-1}. The marked improvement of the GO-hybrid performance is also supported by the promising energy and power density enhancement. Ultimately, our work suggests that ZNC-GO is a propitious and favorable material for supercapacitor electrode.

Acknowledgement

We acknowledge Faculty of Applied Sciences UiTM Shah Alam and UiTM Pahang Jengka Branch for the facilities that have been provided for the research.

References

1. Behnood, R. and Sodeifian, G. (2021). Novel $ZnCo_2O_4$ embedded with S, N-CQDs as efficient visible-light photocatalyst. *Journal of Photochemistry and Photobiology A: Chemistry*, 405: 112971-112983.
2. Balasurya, S. O., Mohammad K., Abdel-maksoud, M. A., Ahamad, S. R., Almasoud, F, AbdElgawad, H., T., Ajith M., Raju, L. L., and Sudheer Khan, S. (2022). Fabrication of Ag-$ZnCo_2O_4$ framework on chitosan matrix for discriminative dual mode detection of S_2- ions and cysteine, and cyto-toxicological evaluation. *Journal of Molecular Liquids*, 347:118356-118367.
3. Kumar, V., Gajraj, V., Gnanasekar, K. I., Dsoke, S., Indris, S., Ehrenberg, H., Roling, B., and Mariappan, C. R. (2021). Hybrid aqueous supercapacitors based on mesoporous spinel-analogous Zn-Ni-Co-O nanorods: Effect of Ni content on the structure and energy storage. *Journal of Alloys and Compounds,* 882:160712-160723.
4. Ahmad, M., Hussain, I., Nawaz, T., Li, Y., Chen, X., Ali, S., Imran, M., Ma, X. and Zhang, K. (2022). Comparative study of ternary metal chalcogenides (MX; M= Zn–Co–Ni; X= S, Se, Te): Formation process, charge storage mechanism and hybrid supercapacitor. *Journal of Power Sources*, 534: 231414-231424.
5. Girija, N., Kuttan, S. S., Jyothibasu, J. P.., Lee, R. H., Nair, B. N., Mohamed, A. A. P., Devaki, S. J., and Hareesh, U. N. S. (2022). Redox participation and plasmonic effects of Ag nanoparticles in nickel cobaltite-Ag architectures as battery type electrodes for hybrid supercapacitor. *Electrochima Acta*, 412:140141-140154.
6. UmaSudharshini, A., Bououdina, M., Venkateshwarlu, M., Manoharan, C., and Dhamodharan, P. A. (2020). Low temperature solvothermal synthesis of pristine Co_3O_4 nanoparticles as potential supercapacitor. *Surfaces and Interfaces*, 19: 100535-100542.
7. Makhlouf, M. Th., Abu-Zied, B. M., and Mansoure, T. H. (2013). Direct fabrication of cobalt oxide nanoparticles employing sucrose as a combustion fuel. *Journal of Nanoparticles*, 2013:1-7.
8. Zhu, Y., Tao, Z., Cai, C., Tan, Y., Wang, A., and Yang, Y. (2022). Facile synthesis Zn-Ni bimetallic MOF with enhanced crystallinity for high power density supercapacitor applications. *Inorganic Chemistry Communications,* 139: 109391-109400.
9. Liu, P., Peng, J., Chen, Y., Liu, M., Tang, W., Guo, Z. H., and Yue, K. (2021). A general and robust strategy for in-situ templated synthesis of patterned inorganic nanoparticle assemblies. *Giant*, 8:100076-100083.
10. Wang, F., Zheng, J., Li, G., Ma, J., Yang, C., and Wang, Q. (2018). Microwave synthesis of mesoporous $CuCo_2S_4$ nanoparticles for supercapacitor applications. *Materials Chemistry and Physics,* 215:121-126.
11. Kumar, A. (2020). Sol gel synthesis of zinc oxide nanoparticles and their application as nano-composite electrode material for supercapacitor. *Journal of Molecular Structure,* 1220: 128654-128663.
12. Belkessam, C., Mechouet, M., Idiri, N., Kadri, A.A., and Djelali, N. E. (2019). Synthesis and characterization of $Ni_{0.3}Co_{2.7}O_4$ oxide nanoparticles immobilized in Teflon cavity electrode for organic pollutants degradation. *Materials Research Express*, 6(10): 1-14.
13. Chen, H., Wang, J., Han, X., Liao, F., Zhang, Y., Han, X., and Xu, C. (2019). Simple growth of mesoporous zinc cobaltite urchin-like microstructures towards high-performance electrochemical capacitors. *Ceramic International*, 45(3): 4059-4066.
14. Gao, K., and Li, S. D. (2020). Hollow fibrous $NiCo_2O_4$ electrodes with controllable Zn

substitution sites for supercapacitors. *Journal of Alloys and Compound*, 832:154927-154935.

15. Wei, X., Chen, D., and Tang, W. (2007). Preparation and characterization of the spinel oxide $ZnCo_2O_4$ obtained by sol-gel method. *Materials Chemistry Physics*, 103(1):54-58.
16. Mustaqeem, M., Naikoo, G. A., Yarmohammadi, M., Pedram, M.Z., Pourfarzad, H., Dar, R. A., Taha, S.A., Hassan, I.U., Bhat, Md Yasir., and Chen, Y.F. (2022). Rational design of metal oxide-based electrode materials for high performance supercapacitors – A review. *Journal of Energy Storage*, 55:105419-105437.
17. Zhang, B., Peng, Z., Song, L., Wu, X., and Fu, X. (2021). Computational screening toward quantum capacitance of transition-metals and vacancy doped/co-doped graphene as electrode of supercapacitors. *Electrochima Acta*, 385:138432-138441.
18. Mohamed, S. G., Attia, S. Y., and Allam, N. K. (2017). One-step, calcination-free synthesis of zinc cobaltite nanospheres for high-performance supercapacitors. *Materials Today Energy*, 4:97-104.
19. Ma, Q., Liu, M., Cui, F., Zhang, J., and Cui, T. (2022). Fabrication of 3D graphene microstructures with uniform metal oxide nanoparticles via molecular self-assembly strategy and their supercapacitor performance. *Carbon,* 204: 336-345.
20. Hosseinkhani, O., Hamzehlouy, A., Dan, S., Sanchouli, N., Tavakkoli, M., and Hashemipour, H. (2023). Graphene oxide/ZnO nanocomposites for efficient removal of heavy metal and organic contaminants from water. *Arabian Journal of Chemistry*, 16(10):105176.
21. Deepi, A., Srikesh, G., and Nesaraj, A. S. (2018). One pot reflux synthesis of reduced graphene oxide decorated with silver/cobalt oxide: A novel nano composite material for high capacitance applications. *Ceramics Internaional*, 44(16): 20524-20530.
22. Iranshahi S., and Mosivand, S. (2022). Cobalt/graphene oxide nanocomposites: Electro-synthesis, structural, magnetic, and electrical properties. *Ceramics International,* 48(9):12240-12254.
23. Merabet, L., Rida, K., and Boukmouche, N. (2018). Sol-gel synthesis, characterization, and supercapacitor applications of MCo_2O_4 (M = Ni, Mn, Cu, Zn) cobaltite spinels. *Ceramics International*, 44(10): 11265-11273.
24. Ya'Aini, N., Pillay Al Gopala Krishnan, A., and Ripin, A. (2019). Synthesis of activated carbon doped with transition metals for hydrogen storage. *E3S Web of Conferences*, 90: 01016-01027.
25. Manoratne, C. H., Rosa, S. R. D., and Kottegoda, I. R. M. (2017). XRD-HTA, UV Visible, FTIR and SEM Interpretation of reduced graphene oxide synthesized from high purity vein graphite. *Material Science Research India*, 14(1): 19-30.
26. Verma, S., Pandey, V. K. and Verma, B. (2022). Facile synthesis of graphene oxide-polyaniline-copper cobaltite (GO/PANI/$CuCo_2O_4$) hybrid nanocomposite for supercapacitor applications. *Synthetic Metals,* 286: 117036-117050.
27. Sagadevan, S., Marlinda, A. R., Johan, M.R., Umar, A., Fouad, H. Alothman, O.Y., Khaled, U., Akhtar, M. S., and Shahid, M. M. S. (2019). Reduced graphene/nanostructured cobalt oxide nanocomposite for enhanced electrochemical performance of supercapacitor applications. *Journal of Colloid and Interface Science*, 558: 68-77.
28. Yang, Y.J., Chen, S., Jiang, C., Yang, P., Wang, N., Cheng, Y., and Liu, M.Y. J. (2022). Hierarchical web-like NiFeMn ternary hydroxides microstructure assembled on reduced graphene oxide for binder-free supercapacitor electrode. *Diamond and Related Materials*, 125: 109009-109020.
29. Acharya, J., Pant, B., Ojha, G. P., Kong, H. S., and Park, M. (2021). Engineering triangular bimetallic metal-organic-frameworks derived hierarchical zinc-nickel-cobalt oxide nanosheet arrays@reduced graphene oxide-Ni foam as a binder-free electrode for ultra-high rate performance supercapacitors and methanol electro-oxidation. *Journal of Colloid and Interface Science*, 602: 573-589.
30. Gedi, S., Manne, R., Manjula, G., Reddy, L. V., Reddy, C. P., Marraiki, N., Kim, W. K., Mallikarjuna, K., and Pratap Reddy, M. (2022). Tunability of the self-assemblies of porous

polygon-like zinc cobaltite architectures using mixed solvents for high-performance supercapacitors. *Journal of Physics and Chemistry of Solids*, 163: 110587-110594.

31. Xu, R., Lin, J., Wu, J., Huang, M., Fan, L., Xu, Z., and Song, Z. (2019). A high-performance pseudocapacitive electrode material for supercapacitors based on the unique $NiMoO_4$/NiO nanoflowers. *Applied Surface Science*, 463:721-731.
32. Huang, B., Tang, Q., Liang, C., Liu, N., and Wang, Y. (2021). Facile synthesis of multilayer graphene nanoplatelets/$ZnCo_2O_4$ microspheres with enhanced performance for asymmetric supercapacitors. *Materials Letters*, 298: 130022-130027.
33. Tseng, C. C., Lee, J. L., Liu, Y. M., Der Ger, M., and Shu, Y. Y. (2013). Microwave-assisted hydrothermal synthesis of spinel nickel cobaltite and application for supercapacitors, *Journal of the Taiwan Institute of Chemical Engineers*, 44(3): 415-419.
34. Ramli, N. I. T., Rashid, S. A., Mamat, M. S., Sulaiman, Y., Zobir, S. A., and Krishnan, S. (2017). Incorporation of zinc oxide into carbon nanotube/graphite nanofiber as high-performance supercapacitor electrode. *Electrochimica Acta*, 228:259–267.
35. Krishnan, S. G., Harilal, M., Yar, A., Vijayan, B. L., Dennis, J. O., Yusoff, M. M., and Jose, R. (2017). Critical influence of reduced graphene oxide mediated binding of M (M = Mg, Mn) with Co ions, chemical stability and charge storability enhancements of spinal-type hierarchical MCo_2O_4 nanostructures. *Electrochimica Acta*, 243:119-128.
36. Pore, O. C., Fulari, A. V., Shejwal, R. V., Fulari, V. J., and Lohar, G. M. (2021). Review on recent progress in hydrothermally synthesized MCo_2O_4/rGO composite for energy storage devices. *Chemical Engineering Journal*, 426: 131544-131576.
37. Handayani, M., Mulyaningsih, Y., Aulia Anggoro, M., Abbas, A., Setiawan, I., Triawan, F., Darsono, N., Nugraha Thaha, Y., Kartika, I., Ketut Sunnardianto, G., Anshori, I., and Lisak, Grzegorz. (2022). One-pot synthesis of reduced graphene oxide/chitosan/zinc oxide ternary nanocomposites for supercapacitor electrodes with enhanced electrochemical properties. *Materials Letters*, 314:8-12.
38. Ezeigwe, E. R., Khiew, P. S., Siong, C. W., and Tan, M. T. T. (2020). Mesoporous zinc–nickel–cobalt nanocomposites anchored on graphene as electrodes for electrochemical capacitors. *Journal of Alloys and Compound*, 816:1-8.
39. Lee, K. S., Seo, Y. J., and Jeong, H. T. (2021). Capacitive behavior of functionalized activated carbon-based all-solid-state supercapacitor. *Carbon Letters,* 31:1041-1049.
40. Zhang, H., Lv, Y., Wu, X., Guo, J., and Jia, D. (2023). Electrodeposition synthesis of reduced graphdiyne oxide/$NiCo_2S_4$ hierarchical nanosheet arrays for small size and light weight aqueous asymmetry supercapacitors. *Journal of Alloys and Compound*, 947:169403-169413.